Science Advances
AAAS

Supplementary Materials for

Mechanistic insights into the roles of the UFM1 E3 ligase complex in ufmylation and ribosome-associated protein quality control

Ryosuke Ishimura *et al.*

Corresponding author: Toshifumi Inada, toshiinada@ims.u-tokyo.ac.jp; Nobuo N. Noda, nn@igm.hokudai.ac.jp; Masaaki Komatsu, mkomatsu@juntendo.ac.jp

Sci. Adv. **9**, eadh3635 (2023)
DOI: 10.1126/sciadv.adh3635

This PDF file includes:

Figs. S1 to S7

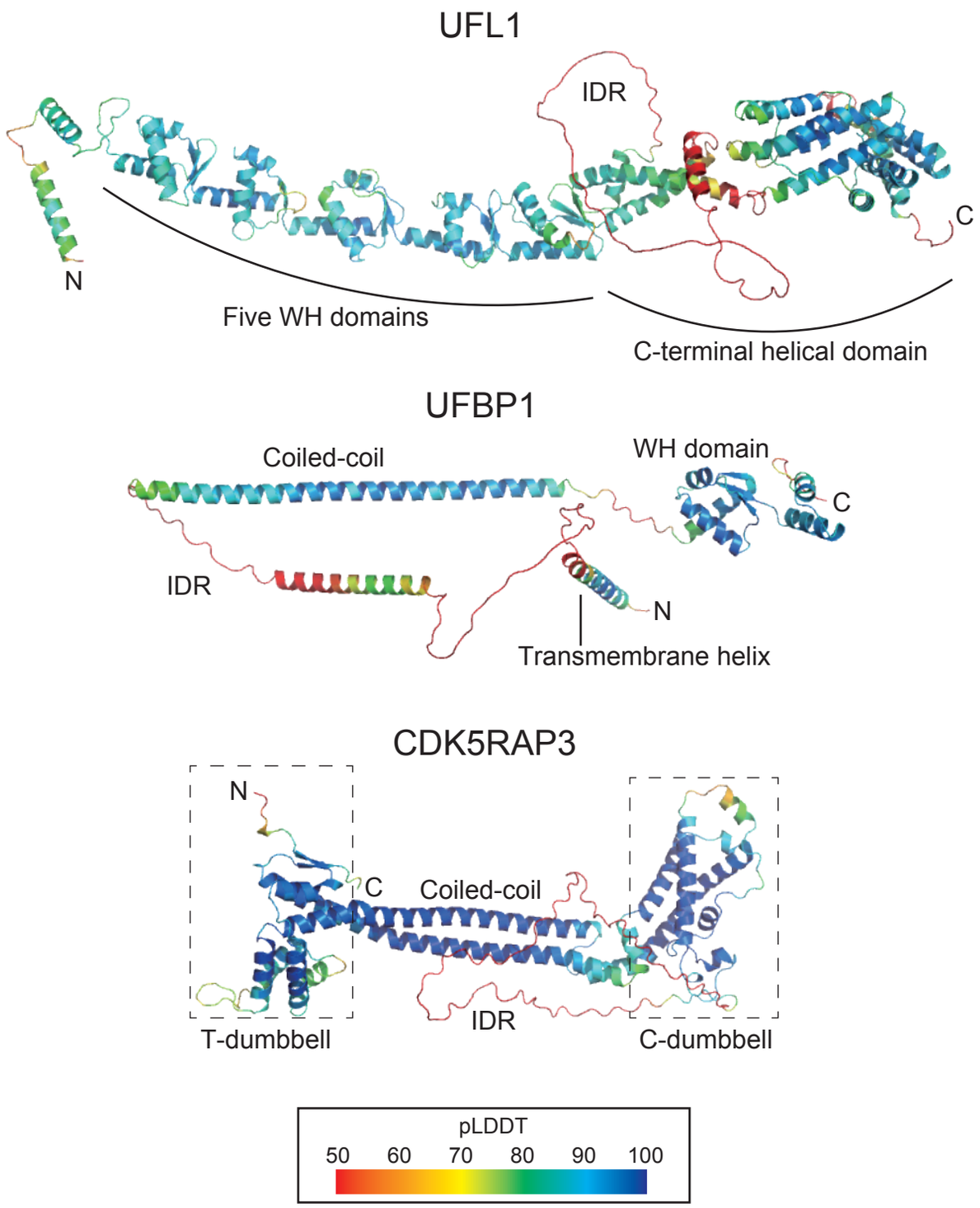

Supplementary Figure S1 Predicted structure of each UFM1 E3 component.
Predicted three-dimensional structures of UFL1 (UniPlot O94874), UFBP1 (UniPlot Q96HY6), and CDK5RAP3 (UniPlot Q96JB5) downloaded from AlphaFold Protein Structure Database. AF2 produces a per-residue confidence score (pLDDT) between 0 and 100, which is indicated by color (the color-score relationship is shown in the box; pLDDT scores between 0 and 50 are colored red).

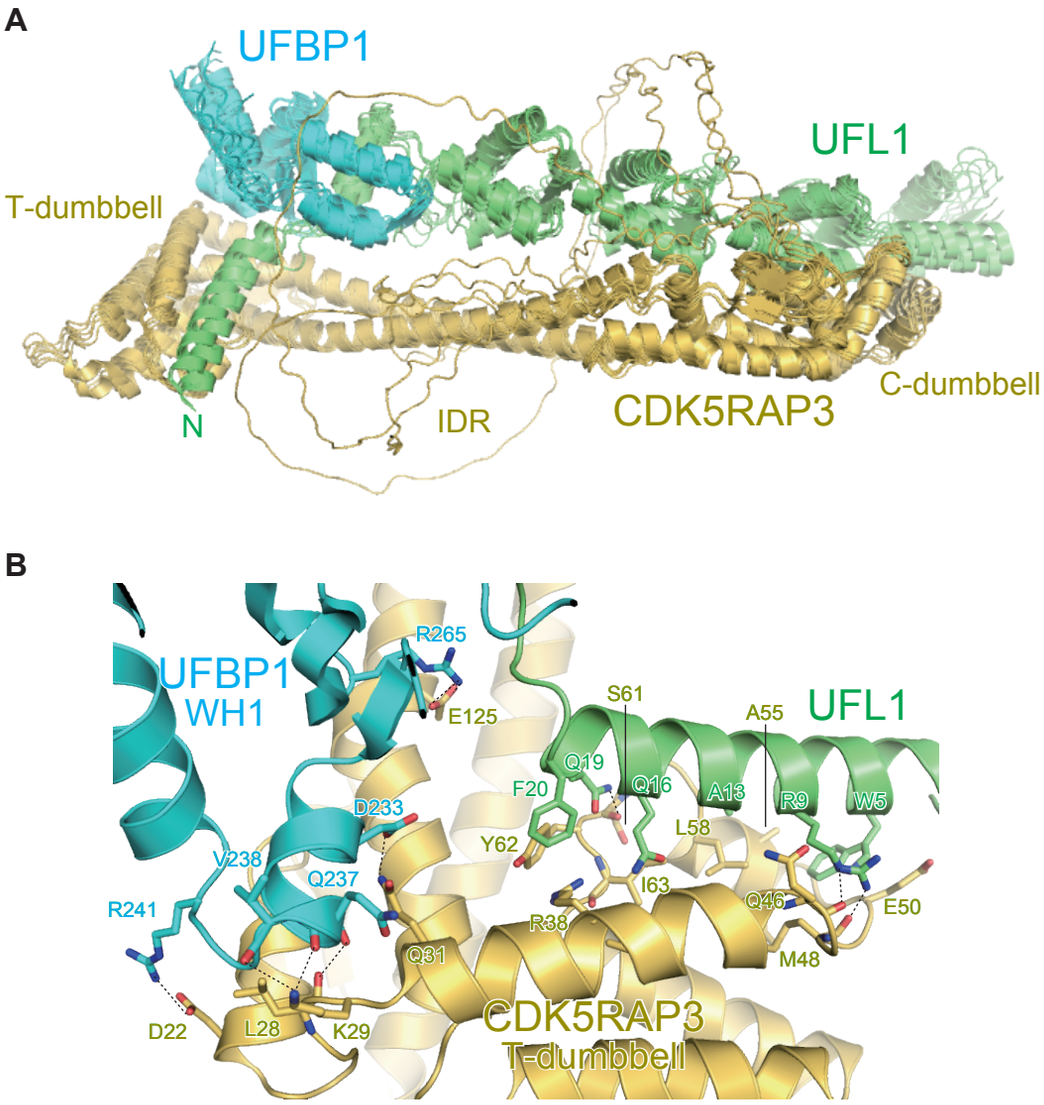

Supplementary Figure S2 Predicted structure of the UFM1 E3 complex.
(A) Predicted three-dimensional structure of the UFL1(1-302)-UFBP1(209-314)-CDK5RAP3 complex by AF2. The top five models are shown superimposed. **(B)** Binding of the T-dumbbell of CDK5RAP3 to the N-terminal helix of UFL1 and the WH1 domain of UFBP1. The side chains involved in this interaction are shown with a stick model, where oxygen and nitrogen atoms are colored red and blue, respectively. Broken lines indicate possible electrostatic interactions.

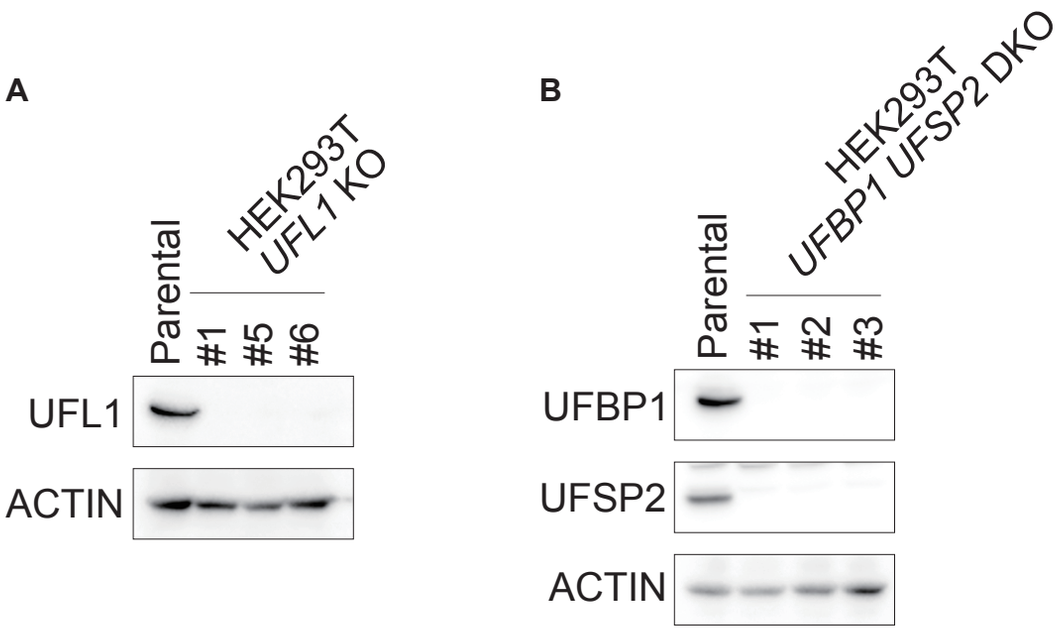

Supplementary Figure S3 Generation of knockout cell lines.
(A-B) Generation of *UFL1* KO (A) and *UFBP1 UFSP2* DKO (B) cell lines. The indicated genotype cell lines were lysed, then subjected to SDS-PAGE followed by immunoblot analysis with the indicated antibodies. Data shown are representative of three separate experiments.

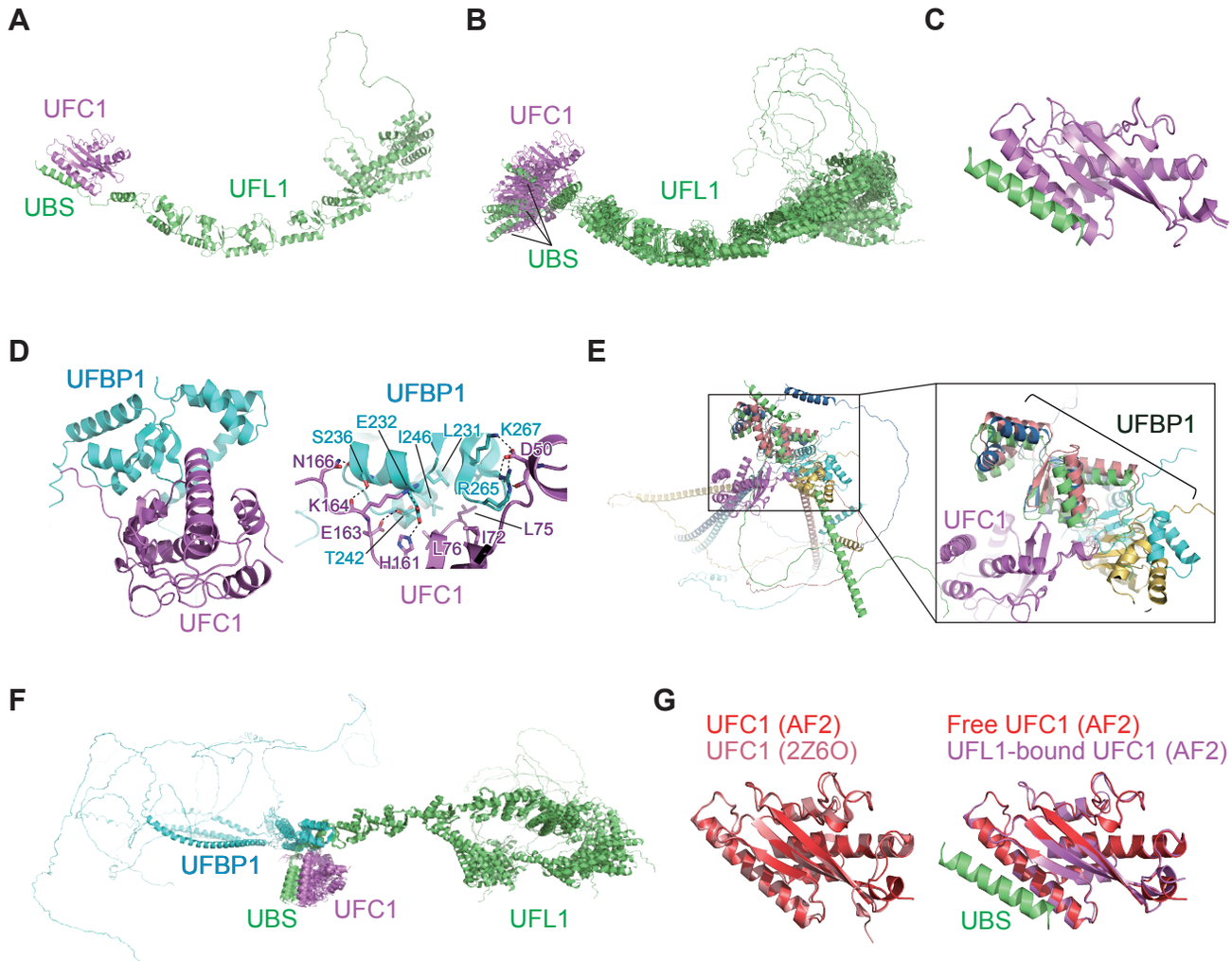

Supplementary Figure S4 Predicted recognition mode of UFM1 E2, UFC1 to E3 subunits.
(A) Top-scored model of the full-length UFL1-UFC1 binary complex predicted by AF2. **(B)** Top five prediction models of the full-length UFL1-UFC1 binary complex are shown superimposed. **(C)** Structural prediction of the UFL1^{UBS}-UFC1 binary complex. Top five models are shown superimposed. **(D)** The top-scoring model of the UFBP1-UFC1 binary complex predicted by AF2. The right panel shows detailed interactions, where the side chains involved in the interaction are shown with a stick model. Oxygen and nitrogen atoms are colored red and blue, respectively. Broken lines indicate possible electrostatic interactions. **(E)** The top five models of the UFBP1-UFC1 binary complex are shown superimposed. **(F)** Structural prediction of the UFL1-UFBP1-UFC1 ternary complex. The top five models are shown superimposed. **(G)** Comparison of the predicted structure of UFC1 (AF2) with the crystal structure (2Z6O) (left). Comparison of the predicted structure of free UFC1 and UFL1^{UBS}-bound UFC1 (right).

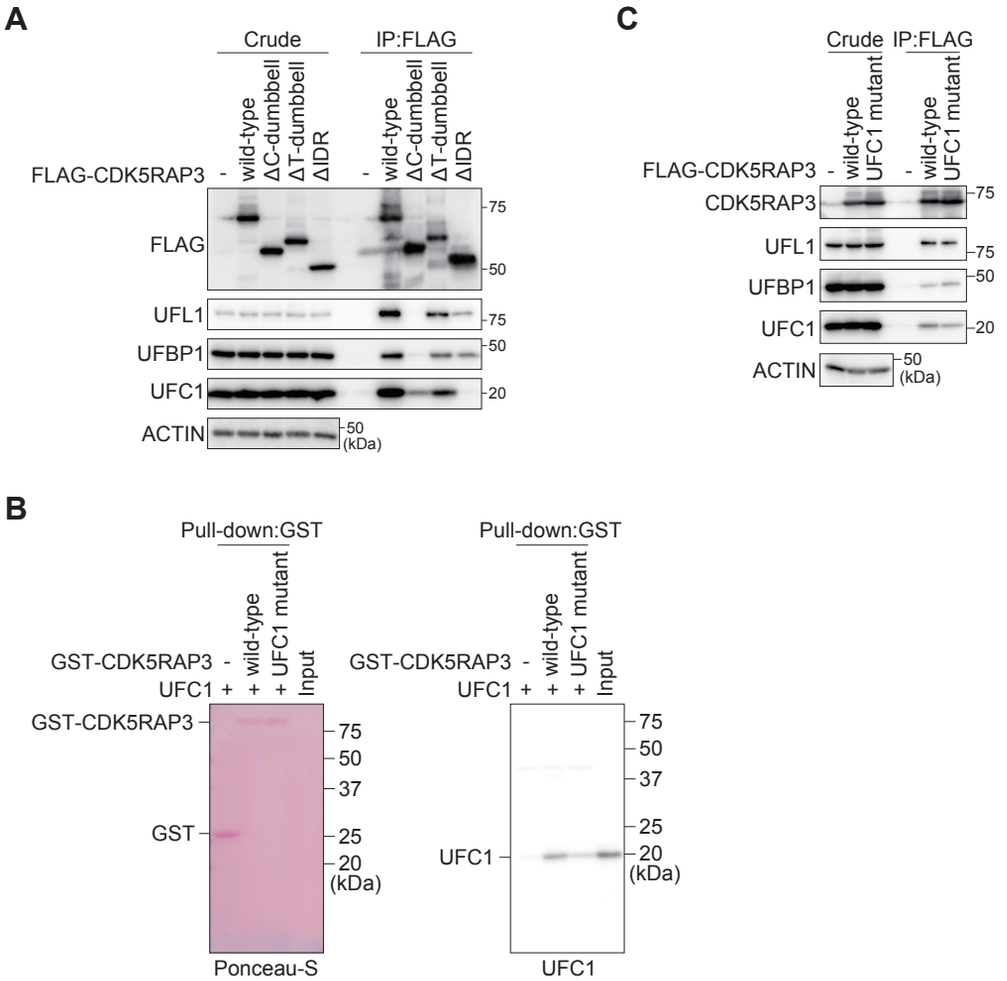

Supplementary Figure S5 CDK5RAP3 interacts with UFC1.
(A) The IDR of CDK5RAP3 is required for its interaction with UFC1. CDK5RAP3 mutants lacking the C-dumbbell (ΔC-dumbbell), T-dumbbell (ΔT-dumbbell), and IDR (ΔIDR) were transfected into *CDK5RAP3*-deficient HEK293T cells. Forty-eight hours after transfection, cells were lysed and immunoprecipitated with anti-FLAG-M2 gel; then, the immunoprecipitants were subjected to immunoblot analysis with the indicated antibodies. **(B)** Direct interaction of CDK5RAP3 with UFC1. GST, GST-CDK5RAP3, or GST-CDK5RAP3$^{I267A\ W269A}$ (CDK5RAP3$^{UFC1\ mutant}$) was immobilized on glutathione Sepharose column. The Sepharose and recombinant UFC1 were incubated, and the supernatant and pulled-down products were then subjected to SDS-PAGE followed by immunoblotting with anti-UFC1 antibody. Data shown are representative of three separate experiments. **(C)** Biochemical characterization of the binding between CDK5RAP3 and UFC1. FLAG-tagged wild-type CDK5RAP3 or CDK5RAP3$^{UFC1\ mutant}$ was transfected into *CDK5RAP3*-deficient HEK293T cells. Forty-eight hours after transfection, cells were lysed and immunoprecipitated with anti-FLAG-M2 gel; then, the immunoprecipitants were subjected to immunoblot analysis with the indicated antibodies. Data shown are representative of three separate experiments.

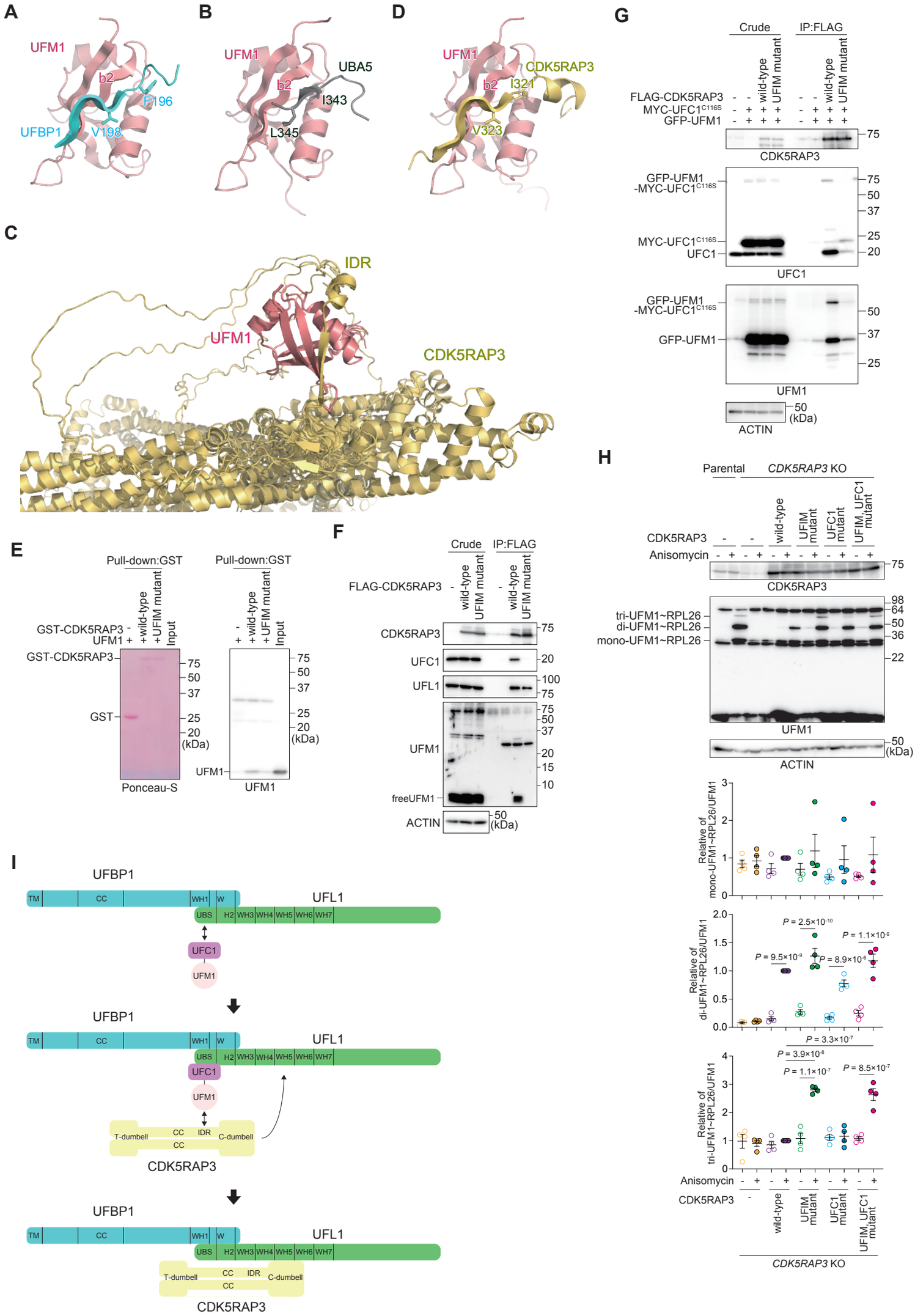
A
UFM1
b2
F196
UFBP1
V198
B
UFM1
UBA5
b2
I343
L345
D
UFM1
CDK5RAP3
b2
I321
V323
C
IDR
UFM1
CDK5RAP3
E
Pull-down:GST
Pull-down:GST
GST-CDK5RAP3
UFM1
wild-type
UFIM mutant
Input
GST-CDK5RAP3
GST
75
50
37
25
20
(kDa)
Ponceau-S
UFM1
UFM1
Pull-down:GST
F
Crude
IP:FLAG
FLAG-CDK5RAP3
wild-type
UFIM mutant
CDK5RAP3
UFC1
UFL1
UFM1
freeUFM1
ACTIN
50
(kDa)
G
Crude
IP:FLAG
FLAG-CDK5RAP3
MYC-UFC1C116S
GFP-UFM1
wild-type
UFIM mutant
CDK5RAP3
GFP-UFM1
-MYC-UFC1C116S
MYC-UFC1C116S
UFC1
UFC1
GFP-UFM1
-MYC-UFC1C116S
GFP-UFM1
UFM1
ACTIN
(kDa)
H
Parental
CDK5RAP3 KO
CDK5RAP3
Anisomycin
wild-type
UFIM mutant
UFC1 mutant
UFIM, UFC1 mutant
CDK5RAP3
tri-UFM1~RPL26
di-UFM1~RPL26
mono-UFM1~RPL26
UFM1
ACTIN
(kDa)
Relative of
mono-UFM1~RPL26/UFM1
Relative of
di-UFM1~RPL26/UFM1
P = 2.5×10-10
P = 1.1×10-9
P = 9.5×10-9
P = 8.9×10-6
P = 3.3×10-7
Relative of
tri-UFM1~RPL26/UFM1
P = 3.9×10-8
P = 1.1×10-7
P = 8.5×10-7
Anisomycin
CDK5RAP3
wild-type
UFIM mutant
UFC1 mutant
UFIM, UFC1 mutant
CDK5RAP3 KO
I
UFBP1
TM
CC
WH1
W
UFL1
UBS
H2
WH3
WH4
WH5
WH6
WH7
UFC1
UFM1
T-dumbell
CC
IDR
C-dumbell
CDK5RAP3

Supplementary Figure S6 CDK5RAP3 interacts with UFM1-charged UFC1.
(A) Crystal structure of UFBP1^{UFIM} bound to UFM1 (PDB 7W3N). **(B)** Crystal structure of UBA5^{UFIM} bound to UFM1 (PDB 5HKH). **(C)** Structural prediction of the CDK5RAP3-UFM1 binary complex. The top five models are shown superimposed. **(D)** Close-up view of the interaction between CDK5RAP3^{UFIM} and UFM1 in the top-scoring model. **(E)** Direct interaction of CDK5RAP3 with UFM1. GST, GST-CDK5RAP3, or GST-CDK5RAP3 UFIM mutant (CDK5RAP3$^{UFIM\ mutant}$) was immobilized on glutathione Sepharose column. The Sepharose and recombinant UFM1 were incubated, and the supernatant and pulled-down products were then subjected to SDS-PAGE followed by immunoblotting with anti-UFM1 antibody. Data shown are representative of three separate experiments. **(F-G)** Biochemical characterization of the binding between CDK5RAP3 and UFM1. (F) FLAG-tagged wild-type CDK5RAP3 or CDK5RAP3^{UFIM} mutant was transfected into *CDK5RAP3*-deficient HEK293T cells. (G) FLAG-tagged wild-type CDK5RAP3 or CDK5RAP3$^{UFIM\ mutant}$, together with MYC-tagged UFC1^{C116S} and GFP-tagged UFM1, were transfected into *CDK5RAP3*-deficient HEK293T cells. Forty-eight hours after transfection, cells were lysed and immunoprecipitated with anti-FLAG-M2 gel; then, the immunoprecipitants were subjected to immunoblot analysis with the indicated antibodies. Data shown are representative of three separate experiments. **(H)** The role of the interaction between CDK5RAP3 with UFM1 on RPL26 ufmylation. Wild-type CDK5RAP3 and UFM1-interaction defective (CDK5RAP3$^{UFIM\ mutant}$), UFC1-interaction defective (CDK5RAP3$^{UFC1\ mutant}$), and double mutant (CDK5RAP3$^{UFIM\ UFC1\ mutant)}$ CDK5RAP3 were transfected in *CDK5RAP3*-deficient HEK293T cells. Forty-eight hours after transfection, the cells were treated with 200 nM anisomycin (Ans) for 1 h and then lysed. The cell lysates were subjected to SDS-PAGE followed by immunoblot analysis with the indicated antibodies. Bar graphs show the results of quantitative densitometric analysis of ufmylated RPL26 (mono-, di-, and tri-ufmylated RPL26) relative to free RPL26 (n = 4). Data are means ± s.e. Statistical analysis was performed by Welch's *t*-test. Data shown are representative of three separate experiments. **(I)** Schematic model of step-wise formation of a five-component complex consisting of the UFBP1-UFL1 E3 complex, UFC1-UFM1 intermediate, and CDK5RAP3.

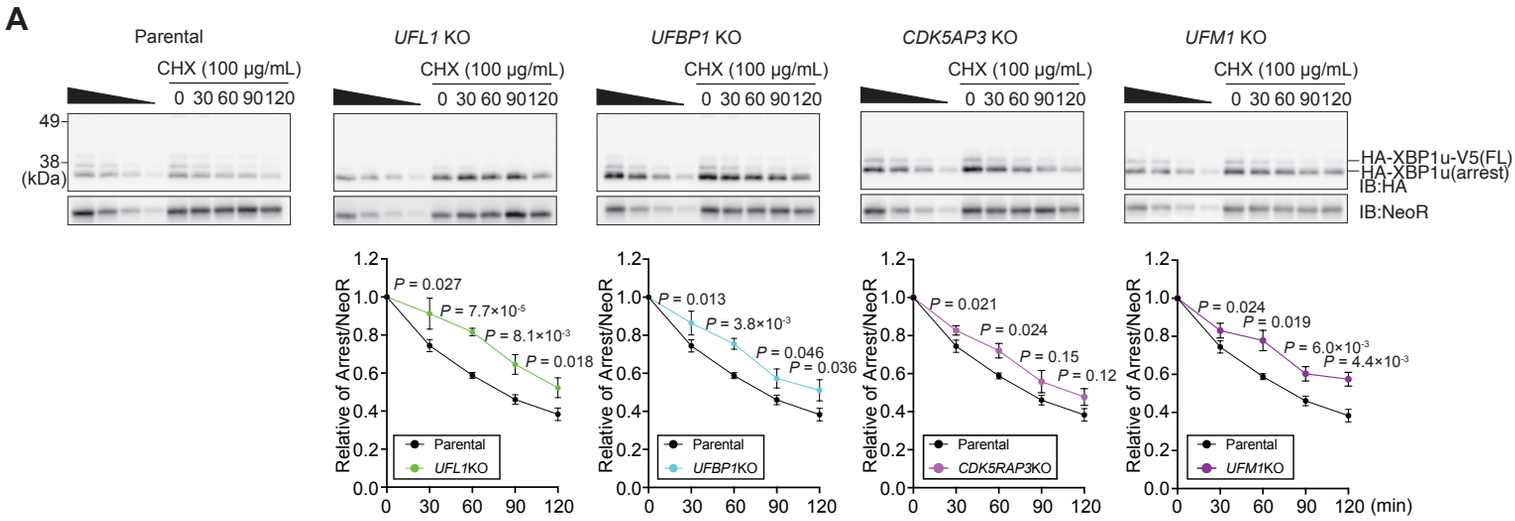

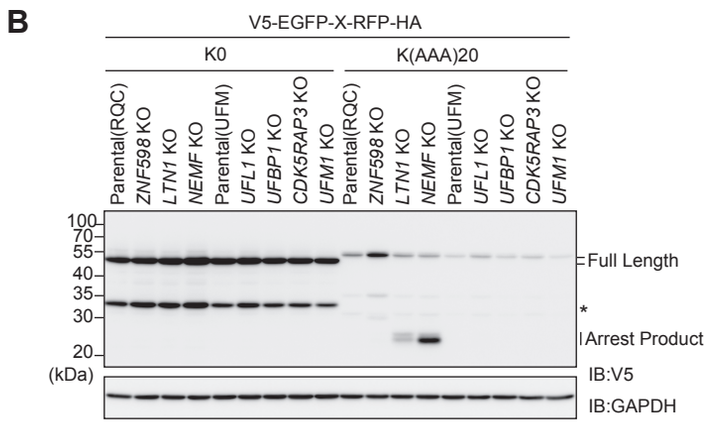

Supplementary Figure S7 The UFM1 E3 complex is required for ER-RQC but not cytosolic-RQC.
(A) UFM1 E3 components are indispensable for ER-RQC. Parental HEK293T cells and indicated KO cells were transfected with the *HA-XBP1u-V5* plasmid. Twenty-four hours after transfection, the cells were treated with cycloheximide (100 μg/mL) for 0, 30, 60, 90, or 120 min, and then lysed. After the cell lysates were treated with RNase, the samples were subjected to neutral PAGE followed by immunoblot analysis with indicated antibodies. Line graphs show the results of quantitative densitometric analysis of arrest product relative to NeoR (n = 5). Data are means ± s.e. Statistical analysis was performed by Welch' s *t*-test. Data shown are representative of three separate experiments. **(B)** UFM1 E3 components are dispensable for cytosolic RQC. The indicated KO cells expressed the *V5-EGFP-K(AAA)0* or *20-RFP-HA* reporter. The cell lysates were subjected to SDS-PAGE followed by western Blotting with antibodies against V5 and GAPDH. The results shown are representative of three separate experiments.